



Trans. Nonferrous Met. Soc. China 35(2025) 3402-3413

Transactions of Nonferrous Metals Society of China

www.tnmsc.cn



Needle-like χ phase precipitation induced by stacking fault in novel Co-based superalloys

Qiu-zhi GAO^{1,2}, Jun-ru WANG^{1,2}, Xu-ming ZHANG^{1,2}, Qing-shuang MA^{1,2}, Song-lin LI^{1,2}, Hui-jun LI^{3,4}, Hong-tao ZHU⁴

- 1. School of Materials Science and Engineering, Northeastern University, Shenyang 110819, China;
- 2. School of Resources and Materials, Northeastern University at Qinhuangdao, Qinhuangdao 066004, China;
 - 3. School of Materials Science and Engineering, Tianjin University, Tianjin 300354, China;
 - 4. School of Mechanical, Materials and Mechatronic Engineering, University of Wollongong, Wollongong, NSW 2522, Australia

Received 22 February 2024; accepted 19 November 2024

Abstract: To explain the precipitation mechanism of χ phase in Co-based superalloys, the microstructural evolution of Co-Ti-Mo superalloys subjected to aging was investigated by X-ray diffraction (XRD), scanning electron microscope (SEM) and transmission electron microscope (TEM). The results show that the needle-like χ phase is mainly composed of D0₁₉-Co₃(Ti,Mo), which is transformed from L1₂- γ' phase, and a specific orientation relationship exists between them. χ phase is nucleated through the shearing of γ' phase due to the influence of stacking fault. The crystal orientation relationship between L1₂ and D0₁₉ can be confirmed as {111}_{L12}//{0001}_{D0₁₉}, and $\langle 112 \rangle_{L12}$ // $\langle 1\overline{100} \rangle_{D0₁₉}$. The growth of D0₁₉- χ phase depends on the diffusions of Ti and Mo, and consumes a large number of elements. This progress leads to the appearance of γ' precipitation depletion zone (PDZ) around D0₁₉- χ phase. The addition of Ni improves the stability of L1₂- γ' phase and the mechanical properties of Co-based superalloys.

Key words: Co-based superalloy; χ phase precipitation; γ' phase; stacking fault; crystal orientation relationship

1 Introduction

Superalloys with excellent high-temperature performances are essential applied materials in the aerospace industry [1,2]. Since 1940s, Ni-based superalloys have been widely used in aerospace γ' phase precipitated strengthening effect in Ni-based superalloys significantly contributes to high-temperature strength and creep properties [3,4]. Compared to Ni, Co has a higher melting point and more excellent oxidation resistance [5], and thus Co-based superalloys are gradually being viewed as the next generation of high-temperature materials with a wide range of application possibilities [6]. Cobased superalloys were believed to lack effective precipitation strengthening, and until 2006, SATO et al [7] discovered γ'-Co₃(Al,W) in the Co-Al-W superalloys. γ'-Co₃(Al,W) phase with L1₂ structure is embedded in face-centered cubic (FCC)-γ matrix [8]. Compared to Ni-based superalloys, the solidus temperature and oxidation resistance of Co-Al-W superalloys are improved [9,10].

The appearance of Co-Al-W superalloys marked an important milestone in the development

of novel Co-based superalloys. However, the microstructural stability of Co-based superalloys at high-temperatures is unsatisfactory due to non-equilibrium nature of γ' precipitates [11,12]. An important concept in the design of novel Co-based superalloys is to substitute W components with other low-density alloy element, while a high dissolution temperature and the stability of γ' phase can still maintain. MAKINENI et al [13] firstly developed a series of W-free Co-based superalloys and expand γ/γ' two-phase region by replacing W elements with Mo, Nb and Ta. PANDEY et al [14] found that the addition of Ti reduces the density while increasing the volume fraction of γ' phase in Co-Al-Mo-Nb-based superalloys. TIRADO et al [15] found that the addition of Ni, Ti, and Al contributes to the formation and the stability of γ' phase, ensuring excellent performance at 850 °C in Co-Ta-V-based alloys.

At present, several studies have been conducted to explore the precipitation mechanism of second phases in Co-based superalloys. Both B₂-CoAl and D0₁₉-Co₃W phases are thermodynamically in equilibrium in Co-Al-W ternary system [16], which are created solely by the decomposition of γ' precipitates. Needle-like χ phase is a detrimental phase, which reduces the mechanical properties of superalloys [17]. Therefore, understanding the precipitation evolution of χ phase is the critical basis for improving the mechanical properties of Co-based superalloys. MA et al [18] found that the precipitation of needle-like χ phase at grain boundaries is significantly restrained by the more addition of Y. Additionally, LI et al [19,20] suggested that the transition from γ' phase to needle-like γ phase is associated with the movement of suitable partial dislocations, while WANG et al [21,22] speculated that needle-like γ phase nucleates at stacking fault sites and then grows with equilibrium composition via atomic diffusion. ZHANG et al [23] investigated the precipitation behavior of D0₁₉ phase in Co-Al-W system using a phase-field model and found that the precipitation time of χ phase advances with increasing temperature.

Currently, the formation mechanism of needle-like χ phase is still unclarified, and most studies have focused on Co–Al–W systems, while less study has been given to W-free Co-based superalloys. Co₃Ti is the only binary stable γ' phase

in commercial Co-based superalloys, and adding Ti to Co-based superalloys holds great potential [24]. In this work, the precipitation of needle-like χ phases that appeared during isothermal aging of Co-Ti-Mo superalloys, with considering the influence of stacking faults, was investigated. In addition, the effect of needle-like χ phase growth on the mechanical properties of Co-Ti-Mo superalloys was also analyzed.

2 Experimental

2.1 Samples preparation

The chemical compositions of experimental materials, Co-13Ti-5Mo and Co-13Ti-5Mo-6Ni, are given in Table 1. Two superalloys were produced by arc melting from pure metals of at least 99.9% in purity in an argon atmosphere. To eliminate elemental segregation in cast superalloys and study microstructural stability of the alloys, the following heat treatments were conducted. The samples were firstly homogenized at 1130 °C for 24 h, cooled in air to room temperature, and then isothermally aged at 800 °C for 24, 64, 128 and 256 h, respectively, followed by cooling to room temperature. To study the effect of different aging temperatures on microstructural evolution, the samples were further isothermal aged at 900 and 1000 °C for 24 and 64 h, respectively.

Table 1 Chemical composition and density of two Co–Ti–Mo-based superalloys

| C11 | Density/ | Composition/at.% | | | |
|-----------------|---------------------|------------------|------|-----|-----|
| Superalloy | $(g \cdot cm^{-3})$ | Co | Ti | Mo | Ni |
| Co-13Ti-5Mo | 8.43 | Bal. | 13.0 | 5.0 | _ |
| Co-13Ti-5Mo-6Ni | 8.33 | Bal. | 13.0 | 5.0 | 6.0 |

2.2 Microstructural characterization

After grinding and polishing, the samples were corroded by electrolytic corrosion with constant voltage of 10 V for 5–10 s in 20% $\rm H_2PO_4$ aqueous solution. The microstructure and precipitates morphologies were characterized by SUPRA55 SAPPHIRE field emission scanning electron microscope (SEM) equipped with energy dispersive spectrometer. Thin slices 0.3 mm thick were intercepted on the treated samples, and then mechanically ground to $50–70~\mu m$. Double spray thinning was performed with a solution of 5%

HClO₄ and 95% CH₃CH₂OH for transmission electron microscopy (TEM; JEM-2100F) characterization with an acceleration voltage of 200 kV. Energy dispersive spectroscopy (EDS) was used to analyze the distribution of alloying elements. X-ray diffraction (XRD) in the 2θ range from 20° to 100° with a scanning rate of 4 (°)/min was performed. The hardness of the samples was tested by MHV-5Z digital Vickers hardness tester with loading of 49 N and holding time of 10 s, 10 random locations were measured, and finally the average values were calculated to ensure the accuracy of hardness value.

2.3 DFT calculations

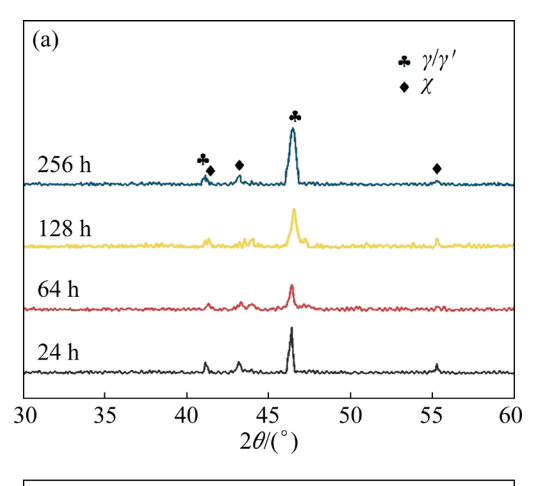
The first-principles calculations were conducted within the framework of density functional theory (DFT) using Vienna Ab Initio Simulation Package (VASP) code. The projectoraugmented wave (PAW) method within the generalized Perdew-Burke-Ernzerhof gradient approximation (GGA) was utilized for the exchange correlation functional. The cut-off energy was set to be 400 eV in every calculation. The k-point sampling grids obtained by using the Monkhorst-Pack method were set to be $6\times6\times1$ for all the interface models. The spin effect was taken into account for all the calculations. A vacuum layer of 15 Å was applied in the slabs and interface models. Ionic relaxation was performed by a conjugate gradient algorithm with the convergence criteria for energy and force set to be $10^{-6} \,\mathrm{eV}$ and $10^{-2} \,\mathrm{eV/Å}$, respectively.

3 Results and discussion

3.1 Microstructures of Co-based superalloys

The phase compositions of Co-13Ti-5Mo and Co-13Ti-5Mo-6Ni superalloys after aging at 800 °C for different time characterized by XRD are shown in Figs. 1(a, b), respectively. It can be found that the phase compositions are stable with duration of aging. Co-13Ti-5Mo and Co-13Ti-5Mo-6Ni superalloys mostly consist of γ/γ' phases and D0₁₉ structure Co₃(Ti,Mo)- γ phase.

Figures 2(a, b) display SEM images of two Co-based superalloys before aging, and typical dendritic structures can be observed. Magnified images of inter-dendritic regions reveal that the inter-dendritic structure is characterized by a γ/γ'



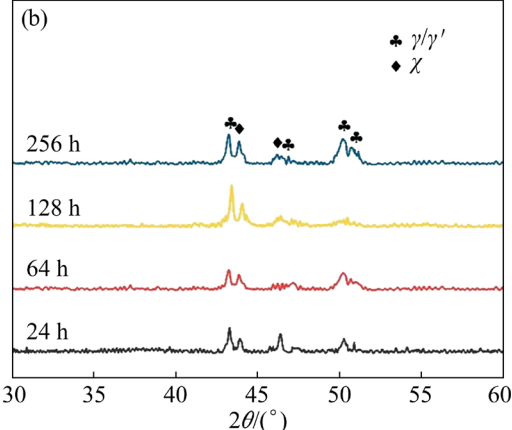


Fig. 1 X-ray diffraction patterns of two Co-based superalloys after aging at 800 °C for different time: (a) Co-13Ti-5Mo; (b) Co-13Ti-5Mo-6Ni

two-phase zone, with γ' phase exhibiting small particle sizes. Additionally, it is also observed that the particle size of γ' phase gradually increases from the center of the inter-dendritic region to its edge. Figures 2(c, d) show microstructures of two superalloys with γ/γ' two-phase after aging. With the increase in aging time, the width of γ phase channel gradually increases, while γ' phase in both Co-based superalloys gradually coarsen. Taking Co-13Ti-5Mo-6Ni superalloy as an example, the statistical data show that the average y phase channel width is $0.03 \mu m$ and the average γ' phase width is 0.1 µm after aging for 24 h, and increase to be 0.04 and 0.23 µm, respectively, after aging for 128 h. Furthermore, the engulfment and growth among adjacent γ' phases can be clearly observed after aging for 256 h, which can be attributed to the diffusions of Ti and Mo from γ' phase into γ matrix with the duration of aging. It should also be noted that the gaps among γ' phases become to be larger, indicating that the redissolution of γ' phase occurs.

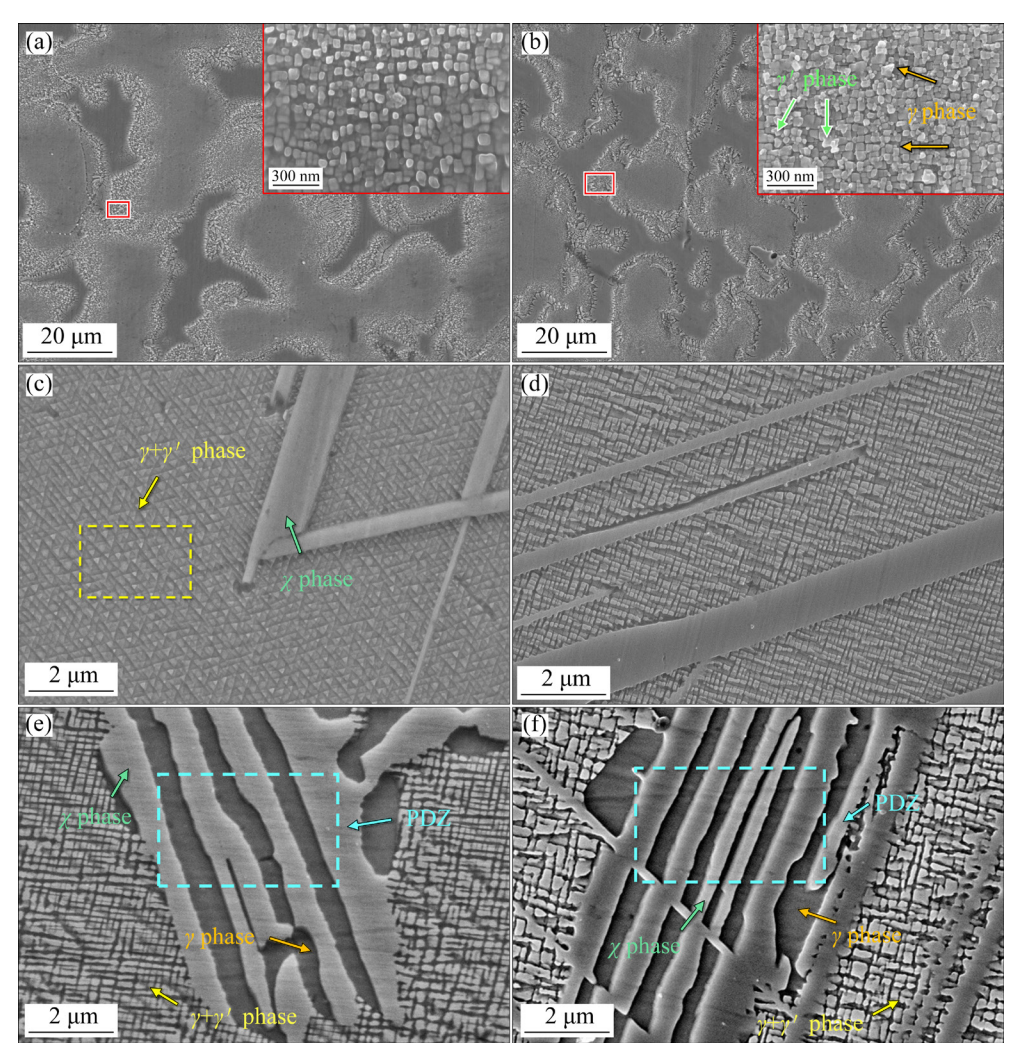


Fig. 2 SEM images of Co-13Ti-5Mo (a, c, e) and Co-13Ti-5Mo-6Ni (b, d, f) superalloys: (a, b) As-cast; (c, d) Aged for 24 h; (e, f) Aged for 256 h

The morphology of γ' phase changes from cubic to elongated with rounded corners, contrasting with the regular square corners of γ' phase observed in Figs. 2(a, b). The morphology of γ' phase remains in its original cubic shape during aging, but the edges become rounded. This can be attributed to two possible reasons. First, the solid solution of alloying elements in γ' phase diffuses into γ matrix. Second, the coarsening of precipitates proceeds towards a lower energy steady state, causing the edge of cubic γ' phase to redissolve [25,26].

Needle-like phases observed after aging are identified as χ phase of D0₁₉ structure with a composition of Co₃(Ti,Mo) based on selected area electron diffraction (SAED) patterns and EDS results. Generally, the χ phase is recognized as a deleterious phase in Co-based superalloys [12,27]. Moreover, needle-like χ phase also coarsens with

the duration of isothermal aging, and its volume fraction increases significantly. It is necessary to investigate the precipitation mechanism of needle-like χ phase because it consumes surrounding alloying elements during coarsening, leading to the appearance of γ' precipitation depletion zone (PDZ) around part of χ phase [17,28,29]. Figures 2(e, f) present large PDZ where γ' phase transforms into χ phase. γ' phase is the main reinforcing phase in Co-based superalloys, and a decrease in the amount of γ' phase inevitably reduces the mechanical properties of superalloys. Therefore, the appearance of large PDZ implies a decrease in comprehensive mechanical properties.

3.2 Phase transformation

Figures 3(a, d) illustrate TEM images of two Co-based superalloys after aging for 24 h. The

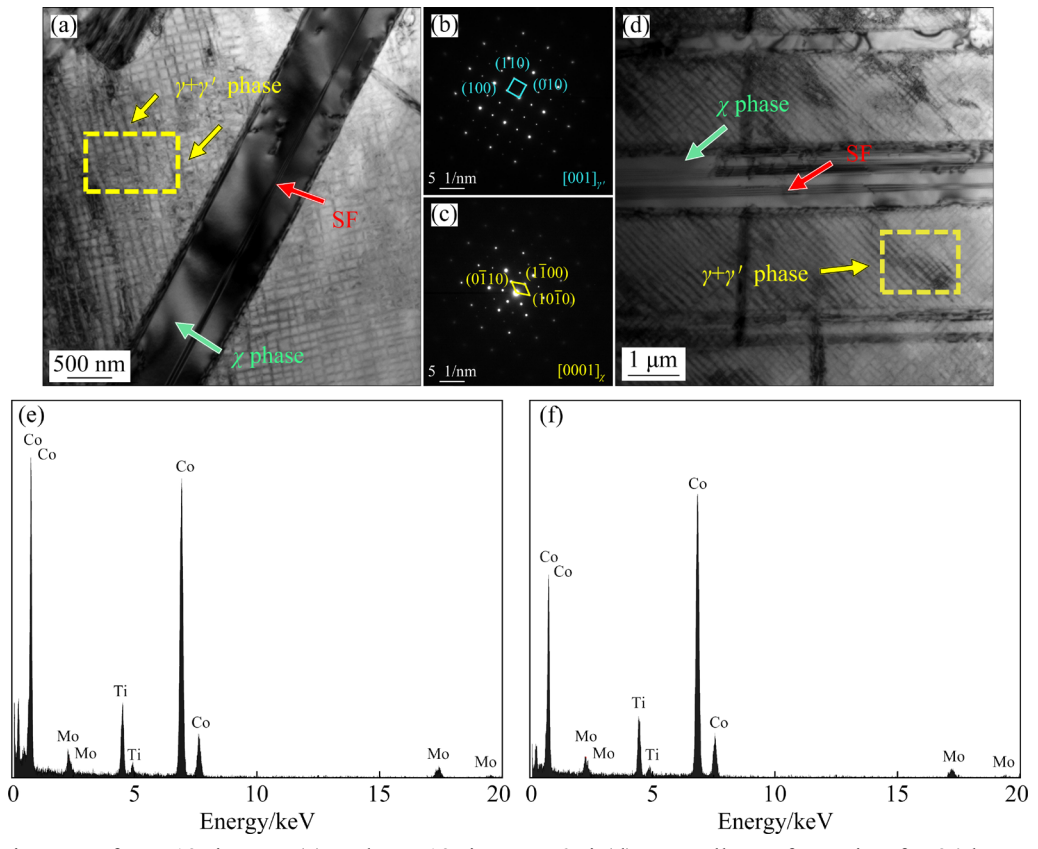


Fig. 3 TEM images of Co-13Ti-5Mo (a) and Co-13Ti-5Mo-6Ni (d) superalloys after aging for 24 h; SAED patterns of γ' (b) and χ (c) phase; EDS results of γ' (e) and χ (f) phase

microstructure of two Co-based superalloys reveals that γ/γ' two-phase regions and needle-like γ phases exist. Furthermore, there are stacking faults (SFs) in needle-like γ phases, which has a same orientation with length direction of χ phase. EDS results for γ' and χ phases are shown in Figs. 3(e, f), and the obtained compositions of γ' and χ phases are listed in Table 2. These results show that γ' and χ phases have same constituent elements and similar contents, and the precipitation of χ phase is likely associated with the lattice structure transformation of γ' phase. During isothermal aging, Mo and Ti diffuse into χ phase, which may cause the appearance of PDZ around the χ phases. Additionally, stacking faults are present in nearly needle-like χ phase, providing evidence that these stacking faults are related to the precipitation of χ phase [30].

Table 2 Chemical compositions of γ' and χ phases

| Phase - | Composition/at.% | | | | |
|---------|------------------|-------|------|--|--|
| | Co | Ti | Mo | | |
| γ' | Bal. | 16.29 | 6.19 | | |
| χ | Bal. | 14.91 | 4.74 | | |

After aging for 128 h, TEM images of two Co-based superalloys are presented in Fig. 4. The microstructure is composed of γ/γ' two-phase regions (indicated by yellow arrows) and needlelike χ phases (indicated by green arrows). Stacking faults can be found in γ/γ' two-phase regions, occurring either across multiple γ' phase particles and γ phase channels or just within γ' phase particles. Additionally, in Figs. 4(c, d), stacking faults can also be observed around needle-like D0₁₉-γ phases. These results suggest that, stacking faults form and increase in γ' phases during isothermal aging. The release of coherent stress during isothermal aging generally results in the development of stacking faults [17]. Furthermore, the formation of $D0_{19}$ - χ phases is associated with formation of stacking faults. After aging for 128 h, the growth of χ phase consumes a large amount of γ' phase forming elements, which leads to the appearance of PDZ as can be seen in Figs. 4(c, d). Consequently, the γ' phase around χ phase disappears, forming two-phase regions comprising only χ phase and γ matrix.

The diffraction pattern calibration of red

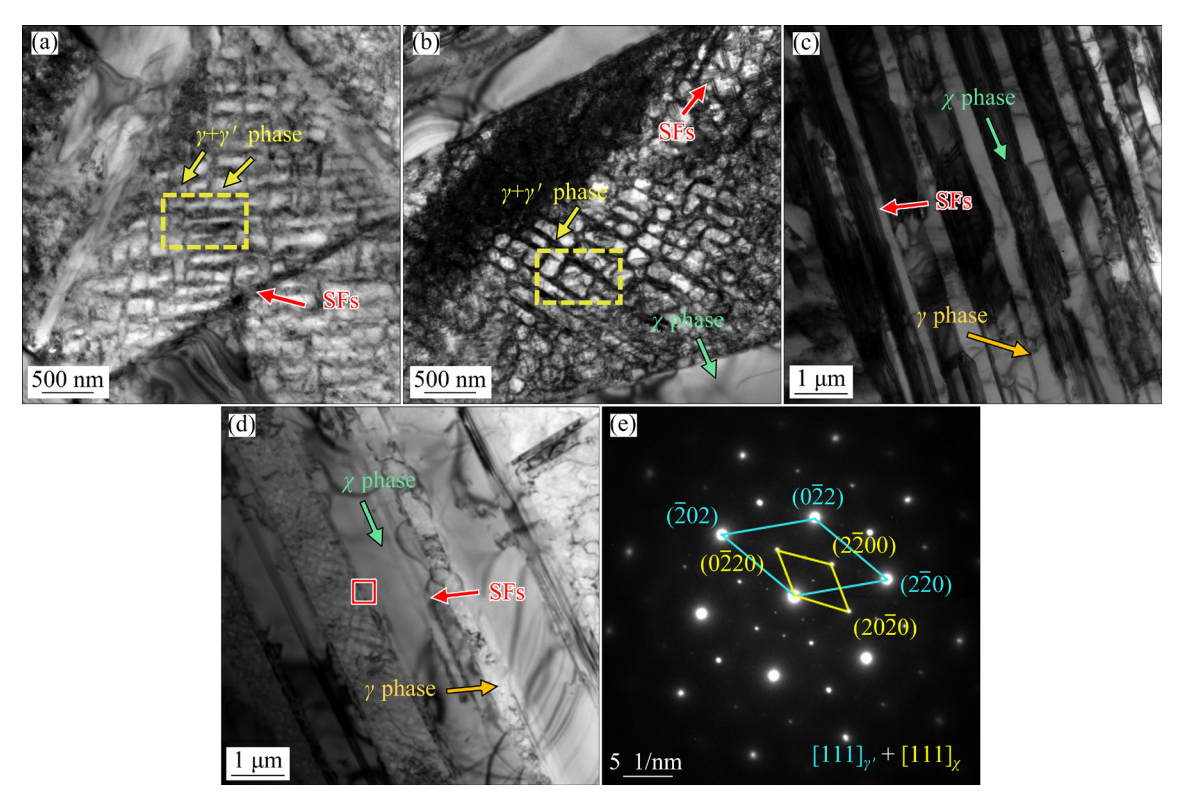


Fig. 4 TEM images of Co-13Ti-5Mo (a, c) and Co-13Ti-5Mo-6Ni (b, d); SAED patterns (e) of χ and γ' phases

rectangular region in Fig. 4(d) is shown in Fig. 4(e), where the SAED patterns of χ and γ' phases are indexed. From Figs. 4(d, e), it can also be seen that a specific orientation relationship exists between $D0_{19}$ - χ phase and $L1_2$ - γ' phase, and their chemical compositions are essentially same. Therefore, it is reasonable to consider that χ phase nucleates through the shearing of γ' phase, as well as the diffusion of Ti and Mo elements [17,19,31]. The schematic diagram of the shearing process is shown in Fig. 5. In Co-based superalloys, γ' phase has an L1₂ structure, with {111} planes stacked in ABCABCABC sequence, and χ phase has D0₁₉ structure, with {0001} planes stacked in an ABABAB... sequence, as shown in Figs. 5(a, b). The schematic diagram of the transition from L1₂ structure to $D0_{19}$ structure is shown in Fig. 5(c). When a C-atomic layer in L1₂ structure slips by $1/3[11\overline{2}]$, a new A-atomic layer can be formed. At this point, the order of the atomic layer changes to CABAABC ... sequence, and a stacking fault is formed at the new A-atomic layer. During aging, a $1/3[11\overline{2}]$ {111} type superlattice intrinsic stacking fault (SISF) is inserted between every two layers of atoms within a certain range of {111} planes of L12 structure [32,33]. The stacking order of atomic

layers in this range changes completely from ABCABC··· sequence to ABABAB··· sequence, with the L1₂ structure disappearing, and a needle-like χ phase formed along the stacking fault. At this point, the transition from L1₂ to D0₁₉ is complete in this local range. Therefore, the crystal orientation relationship between L1₂ and D0₁₉ can be expressed as $\{111\}_{L1/}/\{0001\}_{D0_{19}}$, $\langle112\rangle_{L1/}/\langle1\bar{1}00\rangle_{D0_{19}}$.

The formation of a stacking fault perpendicular to the {111} plane requires the integral movement of new atomic layers, making the expansion of stacking fault more difficult. On the other hand, the expansion of stacking fault along the longitudinal direction on {111} plane only requires a pair of incomplete dislocations moving to opposite directions, which results in relatively easy expansion along the longitudinal direction. Consequently, the morphology of $D0_{19}$ - χ phase usually appears needle-like or rod-like as observed in SEM and TEM images because its coarsening rate in the lateral direction is relatively slow.

The previous first-principles calculations demonstrated that the cohesive energies of L1₂-Co₃(Ti,Mo) and D0₁₉-Co₃(Ti,Mo) are -8.003 and -8.054 eV/atom, respectively. The small energy difference indicates the possibility of a transition

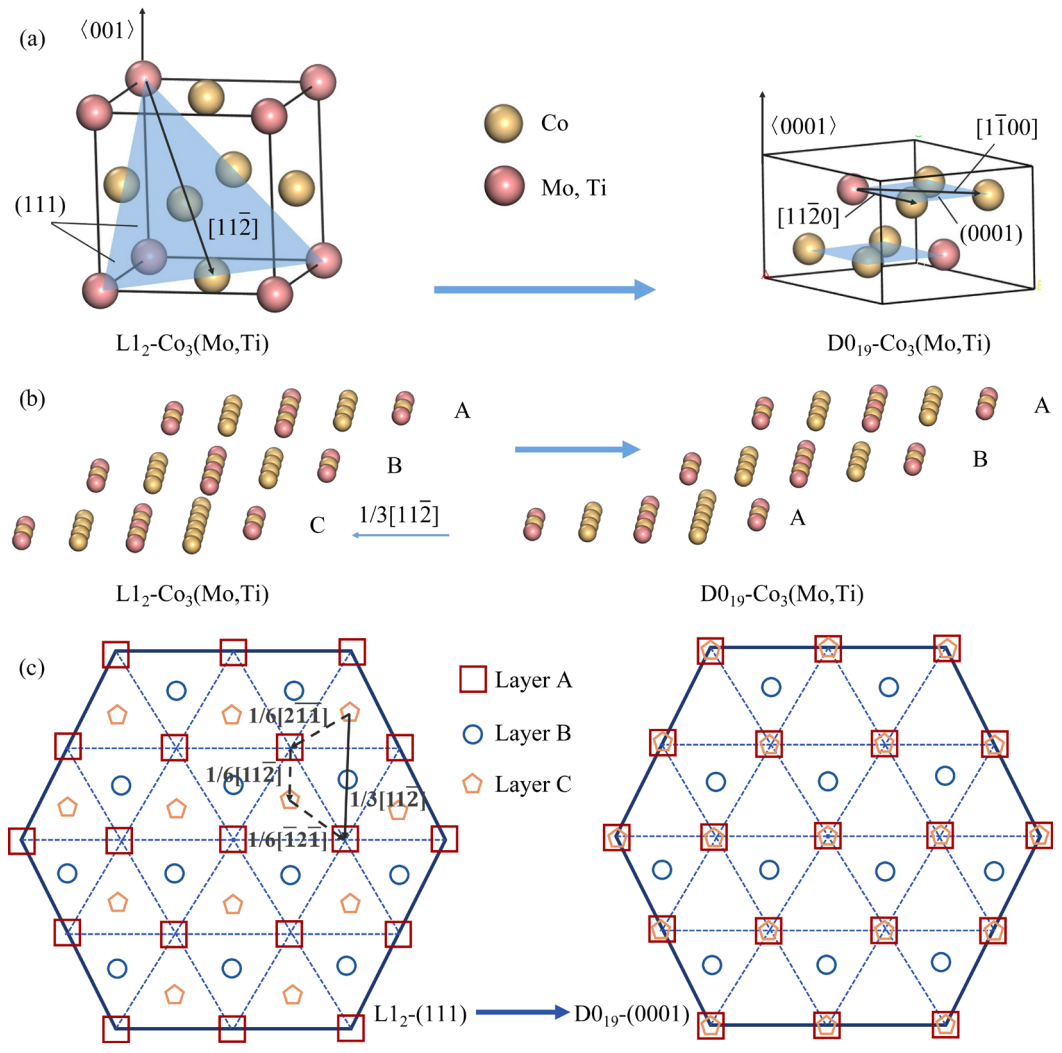


Fig. 5 Schematic diagram of transition of χ phase: (a) Crystal structure and phase transition; (b) C-atomic layer slippage; (c) Intrinsic stacking faults inserting during transformation

from L₁₂ to D₁₉ [34]. However, this transition is not spontaneous, and the driving force is derived from the release of coherent stress during isothermal aging. A new A-atomic layer can be when a C-atomic layer 1/3[112]. Both theoretical calculations experimental observations reveal that 1/3[112] full dislocation is stable and poorly movable, making it difficult to complete the shift directly [19,35,36]. Therefore, the displacement of $1/3[11\overline{2}]$ relies on the joint of multi-step incomplete dislocation movements. This indicates that D0₁₉ structure is difficult to form at plane defects such as stacking faults during the transformation of L12 structure into D0₁₉ structure; conversely, is easy to begin with a core of movable dislocations. The insertion of SISF at {111} crystal plane during transition is shown in Fig. 5(c). C-atomic layer undergoes a displacement of $1/6[2\overline{11}]$, then it goes through two additional displacements of $1/6[11\overline{2}]$ and $1/6[\overline{12}\overline{1}]$, and finally merges into the displacement of $1/3[11\overline{2}]$, at which C-atomic layer reaches A-atomic layer position [31,37]. C-atomic layer is eventually converted into A-atomic layer and a stacking fault is formed. The schematic diagram of three actual displacements and the total displacements by superposition are shown in Fig. 5(c) with dashed and solid arrows, respectively.

3.3 Effect of high-temperature aging

Figure 6 shows microstructures of Co–13Ti–5Mo superalloys aged at different temperatures. As the aging temperature rises, more needle-like χ phases can be observed, and the sizes also increase. Accordingly, as the aging time increases, the growth direction of χ phase becomes to be more

heterogeneous. Firstly, the χ phase is transformed from γ' phase by slippage of stacking fault. Subsequently, new stacking faults occur around the newly expanded χ phase, further resulting in an increase in the number of χ phases.

The production of stacking faults in superalloys is caused by the release of coherent stresses during isothermal aging. Stacking fault energy is temperature-dependent, higher temperatures increase the stacking fault energy, and thus this effect theoretically hinders the development of stacking fault [38]. Initially, stacking faults mostly appear in γ matrix channels, and then expand to γ' phase. The increase in aging temperature reduces the thermal stability of γ' phase, causing it to decompose more quickly [19]. Figure 7 shows that the improvement of aging temperature promotes

back dissolution of γ' phases, and accelerates the annexation and growth among locations near γ' phases, resulting in wider γ matrix channels. Consequently, wider γ matrix channels are more useful to the rapid formation of stacking faults, and further promote the decomposition of γ' phase. Factually, these two processes promote each other and accelerate structural changes in γ' phase.

The growth of χ phase is mainly dependent on the diffusion of Ti and Mo elements [31]. The dislocations, as diffusion channels, accelerate the movement of atoms in γ' phase, which contributes to the growth and coarsening of χ phase. The needle-like χ phase causes stress concentration and a large difference in diffusion potential, promoting the continuous transformation of γ' phase to χ phase [39]. Generally, the growth of χ phase is

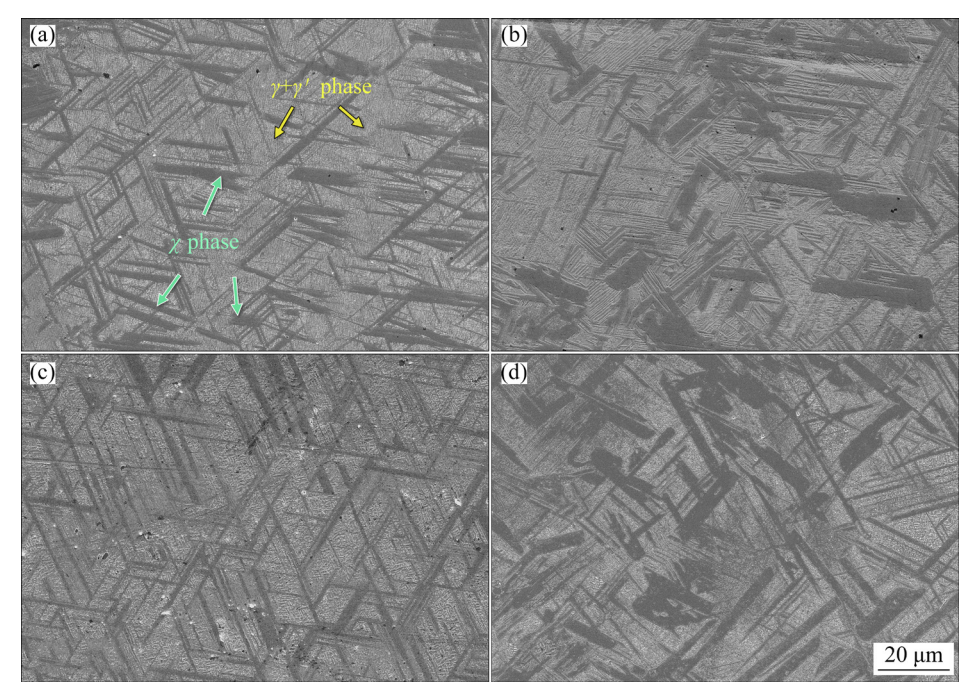


Fig. 6 SEM images showing microstructures of Co-13Ti-5Mo superalloys after different aging processes: (a) 900 °C, 24 h; (b) 900 °C, 64 h; (c) 1000 °C, 24 h; (d) 1000 °C, 64 h

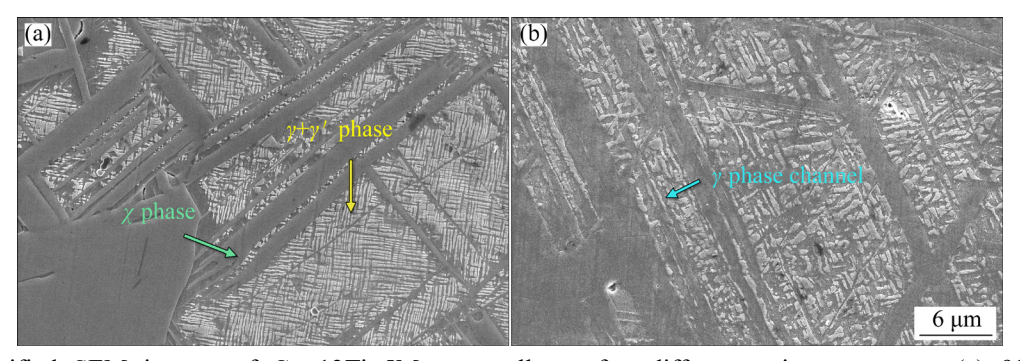


Fig. 7 Magnified SEM images of Co-13Ti-5Mo superalloys after different aging processes: (a) 900 °C, 24 h; (b) 1000 °C, 24 h

accompanied by elemental diffusion during Ostwald ripening, which broadens the interface width of γ/γ phase [23]. With the increase in aging temperature, the diffusion progress becomes to be fast, resulting in high molecular diffusion rate. In fact, larger precipitates and border PDZ around χ phase can be formed with increasing aging temperatures. At higher temperature, the thermodynamic driving forces for the nucleation and growth of D0₁₉ phase are reduced due to increased effect of free energy. However, higher temperatures also increase the mobility of atoms, and thus accelerate the rate of growth and the overall transformation kinetics [40]. As a result, as aging temperatures rise, the number and size of χ phases increase, simultaneously accompanied with γ' phase coarsening and back dissolution as well as the broadening of γ matrix channel.

Compared with the conventional Co-Al-W superalloys after aging [19], the number of needlelike χ phases of Co-Ti-Mo alloys significantly increases, which is related to the addition of Mo elements. The interface energy and atomic diffusion between precipitates and matrix play important roles in the nucleation and growth of needle-like χ phase. According to previous reports, the needlelike χ phase in Co-Ti-Mo is stabilized by Ti element [41], but the driving force required for Ti to diffuse from γ matrix to needle-like χ phase is high, and thus the role of Ti in promoting the growth of needle-like χ phases is weak [42]. Mo can effectively increase the yield strength of alloys, result in excellent mechanical properties in Co-Ti-Mo superalloys. However, for γ/γ' interface, the addition of Mo increases the surface energy, which reduces the stability of interface and promotes the formation of L1₂-Co₃(Ti,Mo) phase, and Mo also increases the stability of needle-like χ phase [35]. In this case, it can be considered to add a certain content of Al to offset part of the impact of Mo and improve the high-temperature stability of superalloys.

The Vicker hardnesses of Co–13Ti–5Mo and Co–13Ti–5Mo–6Ni superalloys after isothermal aging at 800 °C with different time are shown in Fig. 8. It can be seen that Vicker hardnesses of both superalloys decrease with duration of isothermal aging, which can be attributed to two factors. First, the size of γ' phase becomes to be larger, and γ phase channel becomes to be wider, both of which

reduce the precipitation strengthening effect of γ' phase. Second, the formation of χ phase increases, which consumes more Ti and Mo, leading to the formation of PDZ. Consequently, the mechanical properties of superalloys are significantly reduced. In addition, it can be clearly found that Vicker hardness of Co-13Ti-5Mo-6Ni is always higher than that of Co-13Ti-5Mo, which can be attributed to the fact that the addition of Ni can increase the volume fraction of γ' phase, enhancing the precipitation strengthening effect of γ' phase. Furthermore, Ni can also increase complex stacking fault (CSF) energy and anti-phase boundary (APB) energy of L1₂ precipitate on (111) surface, improving microstructural stability and mechanical properties of superalloys [43].

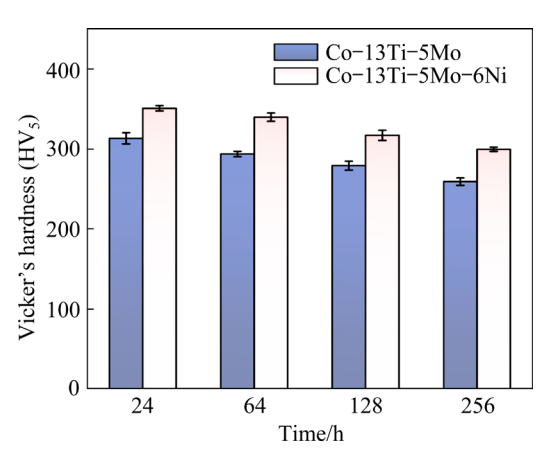


Fig. 8 Vicker hardnesses of two superalloys after aging for different time

To further study the influence of Ni on the stability of superalloys, (111) surface was applied to building a slab model with 40 atoms. The same Co sites in the matrix near $D0_{19}/\gamma$ interface were replaced to investigate the role of Ni distribution at interface between χ phase and γ phase on the work of separation (W_{sep}). The W_{sep} is closely related to structure and properties of the interface and can be used to estimate binding strength and stability of the interface. The W_{sep} can be defined as the reversible work required to separate a single interface into two free surfaces and can be calculated by the following equation [44]:

$$W_{\text{sep}} = (E_{\text{Co,Ti}} + E_{\text{Co}} - E_{\text{slab}})/A$$
 (1)

where E_{slab} is the total energy of interfacial structure; $E_{\text{Co}_3\text{Ti}}$ and E_{Co} are the total energies of Co₃Ti (0001) and Co (111) segregated surface, respectively; A is the interfacial area.

The substituted Co sites are divided into two cases, as seen in Fig. 9(a). One is near location of Ti (75% probability based on equivalent position analysis) and the other is near location of Co (25% probability). The calculation results are shown in Fig. 9(b). These results show that $W_{\rm sep}$ of the interface without Ni is 4.09 J/m². When Ni is at Site 1 and Site 2, $W_{\rm sep}$ values are 4.08 and 4.03 J/m², respectively. In either case, Ni can reduce $W_{\rm sep}$ and stability of system, which inhibits the formation of χ phase.

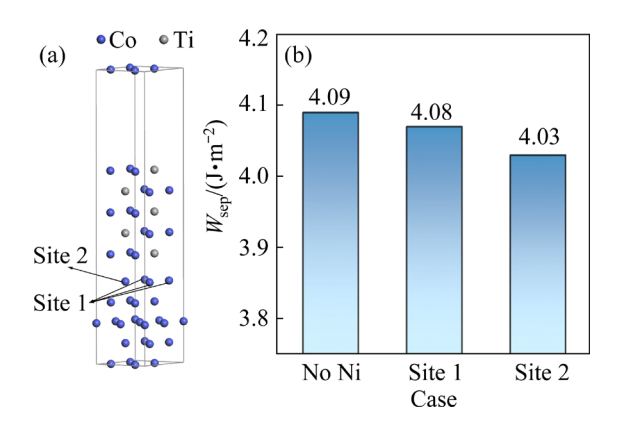


Fig. 9 Stability calculations of χ/γ interface systems: (a) Various sites in γ phases replaced by Ni; (b) W_{sep} in different interface systems

Totally, the slip of stacking faults is the main mechanism of χ phase formation. Since the PDZ significantly reduces mechanical properties of superalloys, the avoidance of χ phase precipitation is a reliable path to improve mechanical properties of superalloys. Notably, a higher stacking fault energy barrier can hinder the slip of stacking faults and prevent the formation of χ phase [35–37]. The stacking fault energy barrier of different alloys can be calculated using first-principles, and it can serve as an important basis for the composition design of novel W-free Co-based superalloys [32,33,35–37].

4 Conclusions

- (1) Microstructures of Co–13Ti–5Mo and Co–13Ti–5Mo–6Ni superalloys are typical dendritics with fine and uniformly distributed γ' phase particles among the dendrites.
- (2) The sizes of γ' phase particles gradually increase from inter-dendritic regions to dendritic arms. γ' phase particles coarsen and even merge, but the volume fraction of γ' phase remains to be

relatively high with duration of aging.

- (3) χ phase, consisting of D0₁₉-Co₃(Ti,Mo), is transformed from L1₂-Co₃(Ti,Mo). Several atomic layers on {111} plane of L1₂ slipping by 1/3[11 $\overline{2}$] with respect to previous atomic layer can produce new layers on {0001} plane of D0₁₉. The crystal orientation relationship between L1₂ and D0₁₉ can be expressed as {111}_{L12}//{0001}_{D0₁₉}, and $\langle 112 \rangle_{L12}$ // $\langle 1\overline{1}00 \rangle_{D0₁₉}$.
- (4) The nucleation and growth of needle-like χ phase are dependent on the diffusion of Ti and Mo, and the number of χ phases increases with the increase in aging temperature. The consumptions of Ti and Mo due to the formation of χ phase result in the formation of PDZ which strongly reduces mechanical properties of superalloys. The addition of Ni improves L1₂ phase stability and enhances mechanical properties of superalloys.

CRediT authorship contribution statement

Oiu-zhi GAO: Conceptualization, Data curation, Formal analysis, Funding acquisition, Investigation, Methodology, Project administration, Supervision, Validation, Writing – Original draft, Writing – Review & Jun-ru WANG: Conceptualization, Data curation, Formal analysis, Investigation, Methodology, Writing Original draft; Xu-ming **ZHANG:** Conceptualization, Data curation, Formal analysis, Investigation, Methodology; Qing-shuang Conceptualization, Data curation, Formal analysis, Investigation, Methodology; Song-lin LI: Formal analysis, Investigation, Methodology; Hui-jun LI: Conceptualization, Formal analysis, Funding acquisition, Investigation, Methodology, Project administration, Supervision, Writing - Review & editing; Hong-tao ZHU: Formal analysis, Investigation, Methodology, Software, Writing – Review & editing.

Declaration of competing interest

The authors declare that they have no known competing financial interests or personal relationships that could have appeared to influence the work reported in this paper.

Acknowledgments

The financial supports from the National Natural Science Foundation of China (Nos. 52171107, 52201203), the National Natural Science Foundation of China-Joint Fund of Iron and Steel Research (No. U1960204) and the "333" Talent Project of Hebei Province, China (No. B20221001) are gratefully acknowledged.

References

- [1] HE Huan-sheng, YU Li-ming, LIU Chen-xi, LI Hui-jun, GAO Qiu-zhi, LIU Yong-chang. Research progress of a novel martensitic heat-resistant steel G115 [J]. Acta Metallurgica Sinica, 2022, 58: 311–323.
- [2] GAO Qiu-zhi, LIU Zi-yun, SUN Lin-lin, MA Qing-shuang, ZHANG Hai-lian, BAI Jing, LIN Xiao-ping, YU Li-ming, LI Hui-jun. Review on precipitates and high-temperature properties of alumina-forming austenitic stainless steel [J]. Journal of Materials Research and Technology, 2023, 25: 5372-5393.
- [3] GAO Qiu-zhi, JIANG Yu-jiao, LIU Zi-yun, ZHANG Hai-lian, JIANG Chen-chen, ZHANG Xin, LI Hui-jun. Effects of alloying elements on microstructure and mechanical properties of Co-Ni-Al-Ti superalloy [J]. Materials Science and Engineering A, 2020, 779: 139139.
- [4] XU Yang-tao, LV Xin, MA Teng-fei, LI Huai, WANG Tong-chao. Effect of Ta and Ni on γ' phase morphology and compression behavior of Co-8.8Al-9.8W superalloys [J]. Materials Science and Engineering A, 2022, 839: 142739.
- [5] ZHANG Yu-heng, FU Hua-dong, ZHOU Fan-jian, XIE Jian-xin. Revealing the effect of Al content on the oxidation of γ'-strengthened cobalt-based superalloys [J]. Corrosion Science, 2022, 198: 110122.
- [6] ZHANG Xu-ming, SHANG Hang, GAO Qiu-zhi, MA Qing-shuang, ZHANG Hai-lian, LI Hui-jun, SUN Lin-lin. Coarsening evolution of γ' phase and failure mechanism of Co-Ni-Al-Ti-based superalloys during isothermal aging [J]. Frontiers in Materials, 2022, 9: 863305.
- [7] SATO J, OMORI T, OIKAWA K, OHNUMA I, KAINUMA R, ISHIDA K. Cobalt-base high-temperature alloys [J]. Science, 2006, 312: 90–91.
- [8] TANAKA K, OOSHIMA M, TSUNO N, SATO A, SATO A, INUI H. Creep deformation of single crystals of new Co-Al-W-based alloys with fcc/L12 two-phase microstructures [J]. Philosophical Magazine, 2012, 92: 4011–4027.
- [9] SUZUKI A, POLLOCK T M. High-temperature strength and deformation of γ/γ' two-phase Co–Al–W-base alloys [J]. Acta Materialia, 2008, 56: 1288–1297.
- [10] CHEN You-heng, WANG Cui-ping, HUANG Xiang. Effects of transition metal elements and O on grain boundary energy and strength of Co by the first-principles study [J]. Transactions of Nonferrous Metals Society of China, 2023, 33: 2428–2438.
- [11] LASS E A, WILLIAMS M E, CAMPBELL C E, CAMPBELL C E, MOON K W, KATTNER U R. γ' phase stability and phase equilibrium in ternary Co–Al–W at 900 °C [J]. Journal of Phase Equilibria and Diffusion, 2014, 35: 711–723.
- [12] KOBAYASHI S, TSUKAMOTO Y, TAKASUGI T. Phase equilibria in the Co-rich Co-Al-W-Ti quaternary system [J]. Intermetallics, 2011, 19: 1908–1912.
- [13] MAKINENI S K, NITHIN B, CHATTOPADHYAY K. A new tungsten-free *γ*–*γ*′ Co–Al–Mo–Nb-based superalloy [J]. Scripta Materialia, 2015, 98: 36–39.
- [14] PANDEY P, RAJ A, PRASAD A S, BALER N, CHATTOPADHYAY K. On the effect of Ti addition on microstructural evolution, precipitate coarsening kinetics and mechanical properties in a Co-30Ni-10Al-5Mo-2Nb alloy

- [J]. Materialia, 2021, 16: 101072.
- [15] TIRADO F L R, TAYLOR S, DUNAND D C. Effect of Al, Ti and Cr additions on the $\gamma-\gamma'$ microstructure of W-free Co–Ta–V-based superalloys [J]. Acta Materialia, 2019, 172: 44–54.
- [16] KOBAYASHI S, TSUKAMOTO Y, TAKASUGI T, CHINEN H, OMORI T, ISHIDA K, ZAEFFERER S. Determination of phase equilibria in the Co-rich Co-Al-W ternary system with a diffusion-couple technique [J]. Intermetallics, 2009, 17: 1085-1089.
- [17] ZHANG Yi, FU Hua-dong, ZHOU Xiao-zhou, ZHANG Yu-heng, DONG Hong-biao, XIE Jian-xin. Microstructure evolution of multicomponent γ'-strengthened Co-based superalloy at 750 °C and 1000 °C with different Al and Ti contents [J]. Metallurgical and Materials Transactions A: Physical Metallurgy and Materials Science, 2020, 51: 1755–1770.
- [18] MA Jian-qiang, ZHONG Fei, LI Shu-suo, SHA Jiang-bo. Microstructure and grain boundary morphology evolution of a novel Co-9Al-9W-2Ta-0.02B alloy doped with yttrium [J]. Rare Metals, 2017, 36: 951-961.
- [19] LI Yu-zhi, PYCZAK F, OEHRING M, WANG Li, PAUL J, LORENZ U, YAO Ze-kun. Thermal stability of γ' phase in long-term aged Co–Al–W alloys [J]. Journal of Alloys and Compounds, 2017, 729: 266–276.
- [20] LI Yu-zhi, PYCZAK F, PAUL J, OEHRING M, LORENZ U, YAO Ze-kun. Microstructure evolution in L1₂ hardened Co-base superalloys during creep [J]. Journal of Materials Research, 2017, 32: 4522–4530.
- [21] WANG Li, OEHRING M, LI Yu-zhi, SONG Lin, LIU Yong, STARK A, LORENZ U, PYCZAK F. Microstructure, phase stability and element partitioning of *γ*–*γ'* Co–9Al–9W–2X alloys in different annealing conditions [J]. Journal of Alloys and Compounds, 2019, 787: 594–605.
- [22] WANG Li, OEHRING M, LORENZ U, YANG Jun-jie, PYCZAK F. Influence of alloying additions on L1₂ decomposition in γ-γ' Co-9Al-9W-2X quaternary alloys [J]. Scripta Materialia, 2018, 154: 176–181.
- [23] ZHANG Xiao-yuan, LI Yong-sheng, SHI Shu-jing, WANG Hui-yu, CHENG Zi-hao. Phase-field simulation of D0₁₉-Co₃W Precipitation in Co-Al-W Superalloys [J]. Metallurgical and Materials Transactions A: Physical Metallurgy and Materials Science, 2022, 53: 2048-2059.
- [24] JIANG Min, JIANG Min, SAREN G, YANG Su-yu, LI Hong-xiao, HAO Shi-ming. Phase equilibria in Co-rich region of Co-Ti-Ta system [J]. Transactions of Nonferrous Metals Society of China, 2011, 21: 2391–2395.
- [25] LIU Jun-ye, YU Jing-jiang, YANG Yun-qiang, ZHOU Yi-zhou, SUN Xaio-feng. Effects of Mo on the evolution of microstructures and mechanical properties in Co-Al-W base superalloys [J]. Materials Science and Engineering A, 2019, 745: 404-410.
- [26] HUANG Yan, WANG Lei, LIU Yang, FU Shun-ming, WU Jian-tao, YAN Ping. Microstructure evolution of a new directionally solidified Ni-based superalloy after long-term aging at 950 °C up to 1000 h [J]. Transactions of Nonferrous Metals Society of China, 2011, 21: 2199–2204.
- [27] KOBAYASHI S, TSUKAMOTO Y, TAKASUGI T. The effects of alloying elements (Ta, Hf) on the thermodynamic stability of γ' -Co₃(Al,W) phase [J]. Intermetallics, 2012, 31: 94–98.

- [28] BAUER A, NEUMEIER S, PYCZAK F, GÖKEN M. Creep strength and microstructure of polycrystalline γ'-strengthened Cobalt-base superalloys [J], Superalloys, 2012, 12: 695–703.
- [29] XUE Fei, WANG Mei-ling, FENG Qiang. Phase equilibria in Co-rich Co-Al-W alloys at 1300 °C and 900 °C [J]. Materials Science Forum, 2011, 686: 388-391.
- [30] KAMALI H, FIELD R D, CLARKE A J, NEDJAD S H, KAUFMAN M J. Development of the γ' stability in Co–Al–W alloys at 800 °C by alloying with carbon [J], Metallurgical and Materials Transactions A: Physical Metallurgy and Materials Science, 2021, 52: 5314–5328.
- [31] CARVALHO P A, BRONSVELD P M, KOOI B J. On the fcc→D0₁₉ transformation in Co−W alloys [J]. Acta Materialia, 2002, 50: 4511–4526.
- [32] MOTTURA A, JANOTTI A, POLLOCK T M. A first-principles study of the effect of Ta on the superlattice intrinsic stacking fault energy of L1₂-Co₃(Al,W) [J]. Intermetallics, 2012, 28: 138–143.
- [33] MOTTURA A, JANOTTI A, POLLOCK T M. Alloying effects in the γ' phase of Co-based superalloys [J]. Superalloys, 2012, 12: 683–693.
- [34] GAO Qiu-zhi, ZHANG Xu-ming, MA Qing-shuang, ZHU Hong-tao, ZHANG Hai-lian, SUN Lin-lin, LI Hui-jun. Accelerating design of novel cobalt-based superalloys based on first-principles calculations [J]. Journal of Alloys and Compounds, 2022, 927: 167012.
- [35] IM H, CHOI W, RYOU K, SEOL J, KANG T, KO W, CHOI P. Enhanced microstructural stability of γ/γ'-strengthened Co-Ti-Mo-based alloys through Al additions [J]. Acta Materialia, 2021, 214: 117011.
- [36] IM H, LEE S, CHOI W, MAKINENI S K, RAABE D, KO W, CHOI P. Effects of Mo on the mechanical behavior of γ/γ'-strengthened Co-Ti-based alloys [J]. Acta Materialia, 2020, 197: 69–80.

- [37] TITUS M, TITUS M S, MOTTURA A, VISWANATHAN G B, SUZUKI A, MILLS M J, POLLOCK T M. High resolution energy dispersive spectroscopy mapping of planar defects in L1₂-containing Co-base superalloys [J]. Acta Materialia, 2015, 89: 423–437.
- [38] ZHAO B, HUANG P, ZHANG Li-bo, LI Su-zhi, ZHANG Ze, YU Qian. Temperature effect on stacking fault energy and deformation mechanisms in titanium and titanium-aluminium alloy [J]. Scientific Reports, 2020, 10: 3086.
- [39] LI Yong-sheng, LONG Hong-li, ZHANG Xiao-yuan, SHI Shu-jing, SANG Peng, ZHANG Zan. Multi-phase-field simulation of D0₁₉-χ transformation in Co–Al–W superalloy with L1₂-γ'+fcc-γ phases [J]. Computational Materials Science, 2023, 230: 112445.
- [40] LI Xin-tong, MA Qing-shuang, LIU En-yu, LI Zhuang-zhuang, BAI-Jing, LI Hui-jun. Phase Order phase transition of HIP nickel-based powder superalloy during isothermal aging [J]. Journal of Alloys and Compounds, 2025, 1010: 177269.
- [41] YU Yan, WANG Cui-ping, LIU Xing-jun, OHNUMA I, KAINUMA R, ISHIDA K. Experimental determination of phase equilibria in the Co-Ti-Mo ternary system [J]. Intermetallics, 2008, 16: 1199-1205.
- [42] JIN Hui-xin, ZHANG Jian-xin, ZHANG Wen-yang, ZHANG You-jian, DU Yi-qun, QIN Jing-yu, WANG Qi. The effects of solutes on precipitated phase/matrix interface stability and their distribution tendencies between the two phases in Co-based superalloys [J]. Computational Materials Science, 2022, 211: 111547.
- [43] CHEN Zheng-hao, KISHIDA K, INUI H, HEILMAIER M, GLATZEL U, EGGELER G. Improving the intermediate- and high-temperature strength of L1₂-Co₃(Al,W) by Ni and Ta additions [J]. Acta Materialia, 2022, 238: 118224.
- [44] LU T, LEE P. Photonic crystal nanofishbone nanocavity [J]. Optics Letters, 2013, 38: 3129–3132.

新型 Co 基高温合金中堆垛层错诱导针状 χ 相析出

高秋志 1,2, 王俊儒 1,2, 张旭明 1,2, 马庆爽 1,2, 李松林 1,2, 李会军 3,4, 朱洪涛 4

- 1. 东北大学 材料科学与工程学院, 沈阳 110819;
- 2. 东北大学 秦皇岛分校 资源与材料学院,秦皇岛 066004;
 - 3. 天津大学 材料科学与工程学院, 天津 300354;
- School of Mechanical, Materials and Mechatronic Engineering, University of Wollongong, Wollongong, NSW 2522, Australia

摘 要: 为了阐明 Co 基高温合金中 χ 相的析出机制,对 Co-Ti-Mo 高温合金进行时效处理,并通过 X 射线衍射、扫描电镜和透射电镜研究其微观结构演变规律。结果表面,针状 χ 相主要由 $D0_{19}$ -Co₃(Ti,Mo)组成,而 $D0_{19}$ -Co₃(Ti,Mo)是由 $L1_2$ - γ '相转变而来,两者具有一定的取向关系。 χ 相通过 γ '相的剪切形核,堆垛层错是 $L1_2$ 结构转变为 $D0_{19}$ 结构的主要诱因。 $L1_2$ 和 $D0_{19}$ 的晶体取向关系可确定为 $\{111\}_{L1_2}$ // $\{0001\}_{D0_{19}}$, $\langle 112\rangle_{L1_2}$ // $\langle 1\overline{100}\rangle_{D0_{19}}$ 。 $D0_{19}$ 相的生长取决于 Ti 和 Mo 元素的扩散,析出会消耗大量元素,导致在 $D0_{19}$ - χ 相周围出现 γ '相耗尽区。Ni 的加入可改善 $L1_2$ - γ '相的稳定性并提高 Co 基高温合金的力学性能。

关键词: Co 基高温合金; χ 相析出; γ '相; 堆垛层错; 晶体取向关系